

Abundance profiles of CH₃OH and H₂CO toward massive young stars as tests of gas-grain chemical models

F.F.S. van der Tak¹, E.F. van Dishoeck¹, and P. Caselli²

¹ Sterrewacht, Postbus 9513, 2300 RA Leiden, The Netherlands

² Osservatorio Astrofisico di Arcetri, Largo E. Fermi 5, 50125 Firenze, Italy

Received 25 April 2000 / Accepted 4 July 2000

Abstract. The chemistry of CH₃OH and H₂CO in thirteen regions of massive star formation is studied through single-dish and interferometer line observations at submillimeter wavelengths. Single-dish spectra at 241 and 338 GHz indicate that $T_{\text{rot}} = 30\text{--}200$ K for CH₃OH, but only 60–90 K for H₂CO. The tight correlation between $T_{\text{rot}}(\text{CH}_3\text{OH})$ and $T_{\text{ex}}(\text{C}_2\text{H}_2)$ from infrared absorption suggests a common origin of these species, presumably outgassing of icy grain mantles. The CH₃OH line widths are 3–5 km s⁻¹, consistent with those found earlier for C¹⁷O and C³⁴S, except in GL 7009S and IRAS 20126, whose line shapes reveal CH₃OH in the outflows. This difference suggests that for low-luminosity objects, desorption of CH₃OH-rich ice mantles is dominated by shocks, while radiation is more important around massive stars.

The wealth of CH₃OH and H₂CO lines covering a large range of excitation conditions allows us to calculate radial abundance profiles, using the physical structures of the sources derived earlier from submillimeter continuum and CS line data. The data indicate three types of abundance profiles: flat profiles at CH₃OH/H₂ ~ 10⁻⁹ for the coldest sources, profiles with a jump in its abundance from ~ 10⁻⁹ to ~ 10⁻⁷ for the warmer sources, and flat profiles at CH₃OH/H₂ ~ few 10⁻⁸ for the hot cores. The models are consistent with the ~ 3'' size of the CH₃OH 107 GHz emission measured interferometrically. The location of the jump at $T \approx 100$ K suggests that it is due to evaporation of grain mantles, followed by destruction in gas-phase reactions in the hot core stage. In contrast, the H₂CO data can be well fit with a constant abundance of a few × 10⁻⁹ throughout the envelope, providing limits on its grain surface formation. These results indicate that $T_{\text{rot}}(\text{CH}_3\text{OH})$ can be used as evolutionary indicator during the embedded phase of massive star formation, independent of source optical depth or orientation.

Model calculations of gas-grain chemistry show that CO is primarily reduced (into CH₃OH) at densities $n_{\text{H}} \lesssim 10^4$ cm⁻³, and primarily oxidized (into CO₂) at higher densities. A temperature of ~ 15 K is required to keep sufficient CO and H on the grain surface, but reactions may continue at higher temperatures if H and O atoms can be trapped inside the ice layer. Assuming grain surface chemistry running at the accretion rate of CO, the observed abundances of solid CO, CO₂ and CH₃OH

constrain the density in the pre-protostellar phase to be $n_{\text{H}} \gtrsim$ a few 10⁴ cm⁻³, and the time spent in this phase to be $\lesssim 10^5$ yr. Ultraviolet photolysis and radiolysis by cosmic rays appear less efficient ice processing mechanisms in embedded regions; radiolysis also overproduces HCOOH and CH₄.

Key words: molecular processes – ISM: molecules – stars: circumstellar matter – stars: formation

1. Introduction

One of the early stages of massive star formation is the “hot core” phase (Kurtz et al. 2000, Macdonald & Thompson 2000), which is characterized by masses of ~ 100 M_⊙ of molecular gas at temperatures of $\gtrsim 100$ K, leading to a rich line spectrum at submillimeter wavelengths like that of the prototypical Orion hot core. The chemical composition of hot cores is quite distinct for its high abundances of fully hydrogenated, large carbon-bearing molecules (Ohishi 1997), as opposed to dark clouds which show predominantly unsaturated species and molecular ions (van Dishoeck & Blake 1998). Saturated carbon chains are not expected in large quantities by steady-state gas-phase models, which led Charnley et al. (1992) and Caselli et al. (1993) to propose models where these molecules are made on dust grains, and evaporate into the gas phase when the newly-formed star heats up its surroundings. This leads to a short period (~ 10⁴ yr) when the envelope of the young star is rich in complex organic molecules. Grain surface reactions at low temperature lead to hydrogenation if atomic H is able to quantum tunnel through activation barriers as proposed by Tielens & Hagen (1982). This model makes specific predictions for the abundance ratios of CO, H₂CO, CH₃OH and their deuterated versions which for a reasonable choice of parameters fit the abundances observed in the Compact Ridge in Orion as shown by Charnley et al. (1997). However, it is unknown if other sources can be fit as well. Alternatively, processing by ultraviolet light or energetic particles may change the ice composition in the vicinity of young stars.

One key molecule to test models of hot core chemistry is methanol, CH₃OH. At temperatures $\lesssim 100$ K, production of CH₃OH in the gas phase goes mainly via radiative association of CH₃⁺ and H₂O, an inefficient process yielding abun-

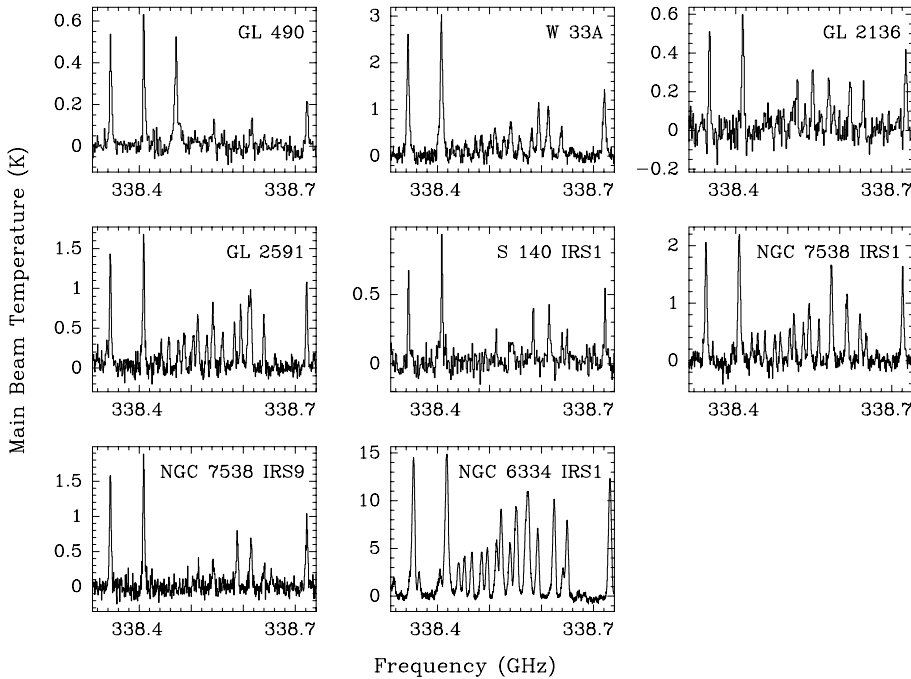


Fig. 1. Spectra of the CH₃OH $J = 7_K \rightarrow 6_K$ transition at 338 GHz, obtained with the JCMT.

dances of only $\sim 10^{-11}$ relative to H₂ (Lee et al. 1996). Observations of CH₃OH toward dark and translucent clouds by Turner (1998) and Takakuwa et al. (1998) yield abundances of $\sim 10^{-9}$, which suggests that grain chemistry operates. Toward the Orion hot core and compact ridge, CH₃OH abundances of $\sim 10^{-7}$ have been observed by Blake et al. (1987) and Sutton et al. (1995), and even higher abundances, $\sim 10^{-6}$, have been inferred from observations of CH₃OH masers (e.g., Menten et al. 1986). Methanol has also been observed in the solid state at infrared wavelengths from the ground by, e.g., Grim et al. (1991) and Allamandola et al. (1992) and recently by Dartois et al. (1999b), at abundances up to 10^{-6} .

To study the organic chemistry in warm (30–200 K) and dense ($10^4 - 10^7 \text{ cm}^{-3}$) circumstellar envelopes, this paper discusses observations of CH₃OH and H₂CO lines at submillimeter wavelengths. Although gas-grain interactions are clearly important for methanol, it is unknown how efficiently (if at all) surface reactions modify the composition of the ices. In addition, it is still open what process returns the molecules to the gas phase: thermal heating, shocks or both? Finally, the ice layer must have formed at temperatures and densities much lower than the present situation, and hence provides a unique fossil record of the conditions in the molecular cloud prior to star formation.

The sources are thirteen massive ($L = 10^3 - 10^5 L_\odot$) stars, which are at an early stage of evolution and still embedded in $10^2 - 10^3 M_\odot$ of dust and molecular gas. A few of the sources are hot cores by the definition of Kurtz et al. (2000), but most are in an even younger phase where most of the envelope is still at low temperatures. The physical structure of the sources has been studied by van der Tak et al. (2000), who developed detailed temperature and density profiles. The wealth of CH₃OH and H₂CO lines, combined with the physical models, allows the determination of abundance profiles for H₂CO and CH₃OH,

which demonstrate that CH₃OH evaporates off dust particles in the envelope on a $\sim 10^{4-5}$ yr time scale, while H₂CO is predominantly formed in the gas phase. The excitation and abundance of CH₃OH are therefore useful evolutionary indicators during the embedded stage of star formation. Moreover, by comparing the observed amounts of evaporated CH₃OH and CO₂ to a model of grain surface chemistry, we set limits on the density and the duration of the pre-protostellar phase.

2. Observations

2.1. Single-dish observations

Spectroscopy of the $J = 5 \rightarrow 4$ and $7 \rightarrow 6$ bands of CH₃OH near 242 and 338 GHz was performed with the 15-m James Clerk Maxwell Telescope (JCMT)¹ on Mauna Kea, Hawaii in May and October of 1995. The beam size (FWHM) and main beam efficiency of the antenna were 18'' and 69% at 242 GHz and 14'' and 58% at 338 GHz. The frontends were the receivers A2 and B3i; the backend was the Digital Autocorrelation Spectrometer, covering 500 MHz instantaneous bandwidth. Pointing was checked every 2 hours during the observing and was always found to be within 5''. To subtract the atmospheric and instrumental background, a reference position 180'' East was observed. Integration times are 30–40 minutes for each frequency setting, resulting in rms noise levels in T_{mb} per 625 kHz channel of ≈ 30 mK at 242 GHz to ≈ 50 mK at 338 GHz. Although the absolute calibration is only correct to $\approx 30\%$, the relative strength of lines within either frequency setting is much more accurate.

¹ The James Clerk Maxwell Telescope is operated by the Joint Astronomy Centre, on behalf of the Particle Physics and Astronomy Research Council of the United Kingdom, the Netherlands Organization for Scientific Research and the National Research Council of Canada.

Table 1. Fluxes $\int T_{\text{MB}}dV$ (K km s⁻¹) and FWHM widths (km s⁻¹) of lines observed with the JCMT.

Line (K,A/E) ^a	Frequency (MHz)	GL 490	W 33A	GL 2136	GL 2591	S 140 IRS1	NGC 7538 IRS1	NGC 7538 IRS9	NGC 6334 IRS1	GL 7009S	IRAS 20126	W 28 A2 ^d
<i>J</i> = 5 → 4 band												
0 E	241700.2	0.8	5.3	0.7	2.0	1.5	4.8	3.0	79.0	1.8	6.4	27.1
-1 E	241767.2	2.7	12.3	0.9	3.3	3.0	8.5	6.7	102.	7.5	4.1	41.6
0 A ⁺	241791.4	3.0	13.8	1.1	4.0	3.5	9.7	7.6	101.	8.5	8.4	39.5
4 A	241806.5	< 0.2	1.2	0.2	0.6	< 0.2	1.2	< 0.2	31.6	< 0.2	2.2	3.0
-4 E	241813.2	< 0.2	0.7	0.2	0.4	< 0.2	0.8	< 0.2	21.4	< 0.2	1.1	0.9
4 E	241829.6	< 0.2	0.8	< 0.2	0.3	< 0.2	1.4	< 0.2	25.5	< 0.2	0.8	2.6
3 A	241832.9	< 0.2	1.9	< 0.2	1.3	0.5	1.6	1.2	36.0	< 0.2	3.2	11.5
3 E / 2 A ⁻	241843.0	0.3	2.2	0.4	1.3	0.5	2.4	0.9	55.4	< 0.2	4.1	12.0
-3 E	241852.3	< 0.2	0.9	< 0.2	0.6	< 0.2	0.9	< 0.2	28.0	< 0.2	1.5	3.6
1 E	241879.0	0.5	3.7	1.0	1.6	1.2	3.5	2.0	57.6	< 0.2	4.4	20.6
2 A ⁺	241887.7	0.2	2.0	0.5	1.0	0.3	1.5	0.6	38.9	< 0.2	2.4	8.2
∓2E	241904.4	0.8	4.8	1.0	2.3	1.5	5.0	2.8	78.3	0.9	5.8	26.1
<i>J</i> = 7 → 6 band												
-1 E	338344.6	2.1	14.1	2.1	5.2	2.1	8.8	6.0	86.8	27.6
0 A ⁺ ^b	338408.6	2.2	17.9	2.8	6.2	2.8	11.3	6.6	128.6	25.7
-6 E	338430.9	< 0.3	1.2	< 0.5	< 0.5	< 0.5	1.4	< 0.5	23.6	< 3
6 A	338442.3	< 0.3	1.4	< 0.5	1.1	< 0.5	1.5	< 0.5	23.7	< 3
-5 E	338456.5	< 0.3	1.6	< 0.5	1.5	< 0.5	1.2	< 0.5	26.2	< 3
5 E	338475.2	< 0.3	1.6	< 0.5	1.5	< 0.5	1.5	< 0.5	29.5	< 3
5 A	338486.3	< 0.3	1.9	< 0.5	1.9	< 0.5	1.6	< 0.5	31.4	< 3
-4 E	338504.0	< 0.3	2.2	< 0.5	1.8	< 0.5	2.0	< 0.5	35.2	< 3
4A / 2A ⁻	338512.7	< 0.3	3.5	1.1	2.8	0.6	3.1	0.8	59.4	11.6
4 E	338530.2	< 0.3	2.3	< 0.5	1.5	< 0.5	2.3	< 0.5	33.3	< 3
3 A	338541.9	0.5	5.2	1.5	3.7	1.3	4.9	1.6	65.7	13.5
-3 E	338559.9	< 0.3	2.6	< 0.5	1.8	< 0.5	2.2	0.4	< 102	< 3
3 E ^c	338583.1	< 0.3	9.2	< 0.5	2.1	1.3	8.1	2.9	39.4	3.8
1 E	338615.0	0.6	7.2	1.3	2.7	1.7	3.1	2.8	57.3	42.5
2 A ⁺	338639.9	0.2	3.7	0.2	2.4	0.6	3.6	1.1	41.1	11.4
∓2E	338722.5	1.0	8.8	2.0	4.0	1.5	6.9	3.9	74.0	24.9
Line Width												
		3.4	5.2	3.0	3.5	2.7	3.9	3.6	5.7	6.9	7.5	6.2
		±0.7	±1.1	±1.3	±0.4	±0.2	±0.6	±0.7	±0.5	±1.3	±1.9	±0.9

^a When no superscript is given for A-type methanol, the A⁺ and A⁻ lines are blended.

^b Blend with K=6 E at 338404.5 MHz, assumed to equal K=-6 E.

^c Possible contribution from K=1 A⁻ at 341415.6 MHz.

^d This source is also known as G 5.89-0.39; 338.5 GHz data are from Thompson & MacDonald 1999.

In addition to these CH₃OH lines, this paper discusses observations of lines of H₂CO, obtained in a similar manner, which were presented in van der Tak et al. (2000). We will also use data on both molecules for W 3 IRS5 and W 3 (H₂O) from the survey by Helmich & van Dishoeck (1997), and CH₃OH *J* = 7 → 6 data from Thompson & MacDonald (1999).

2.2. Interferometric observations

Maps of the $J_K = 3_1 \rightarrow 4_0$ A⁺ (107013.852 MHz; $E_u = 28.01$ K) and $11_{-1} \rightarrow 10_{-2}$ E (104300.461 MHz; $E_u = 157.24$ K) lines of CH₃OH were obtained for four sources in 1995–1999 with the millimeter interferometer of the Owens Val-

ley Radio Observatory (OVRO)². This instrument consists of six 10.4 m antennas on North-South and East-West baselines, and a detailed technical description is given in Padin et al. (1991). For the sources GL 2591, NGC 7538 IRS1 and NGC 7538 IRS9, data were taken in the compact and extended configurations, while for the Southern source W 33A, a hybrid configuration with long North-South but short East-West baselines was also used to improve the beam shape. Antenna spacings range from the shadowing limit out to 90 kλ, corresponding to spatial frequencies of 0.018–0.44 arcsec⁻¹. The observations were carried out simultaneously with continuum observations, which have been

² The Owens Valley Millimeter Array is operated by the California Institute of Technology under funding from the U.S. National Science Foundation (AST-9981546).

Table 2. Beam-averaged column densities and excitation temperatures of CH₃OH and H₂CO, and abundances inferred for a power law envelope using spherical Monte Carlo models.

Source	$N(\text{CH}_3\text{OH})$ cm^{-2}	$N(\text{H}_2\text{CO})$ cm^{-2}	$T(\text{CH}_3\text{OH})$ K	$T(\text{H}_2\text{CO})$ K	$\text{CH}_3\text{OH}/\text{H}_2$ 10^{-9}	$\text{H}_2\text{CO}/\text{H}_2^c$ 10^{-9}
W 3 IRS5	1.6(14)	7.8(13)	73	78	0.4	3
GL 490	3.6(14)	4.3(13)	24	94	1.0	1
W 33A	2.0(15)	1.2(14)	155	88	3.1 / 90 ^b	4
GL 2136	4.4(14)	4.5(13)	143	76	0.9	8
GL 7009S ^a	3.9(15)	...	8	...	0.7	...
GL 2591	1.2(15)	8.0(13)	163	89	2.6 / 80 ^b	4
S 140 IRS1	2.5(14)	8.0(13)	41	60	1.2	5
NGC 7538 IRS1	2.2(15)	1.9(14)	189	87	2.0 / 60 ^b	10
NGC 7538 IRS9	6.5(14)	1.0(14)	29	82	2.3	10
W 3 (H ₂ O)	7.5(15)	5.0(14)	203	181	5.9	3
NGC 6334 IRS1	3.8(16)	1.6(15)	213	193	24.	7
IRAS 20126 ^a	2.2(15)	...	139	...	2.6	...
W 28 A2	4.2(15)	...	43	...	12.	...

^a Only CH₃OH $J = 5 \rightarrow 4$ observed.

^b Abundances in cold ($T < 90$ K) and in warm ($T > 90$ K) gas.

^c From van der Tak et al. 2000.

presented in van der Tak et al. (1999, 2000). We refer the reader to these papers for further observational details.

3. Results

3.1. Submillimeter spectroscopic results

Fig. 1 presents the calibrated JCMT spectra, reduced using the IRAM CLASS package. All lines are due to either A- or E-type CH₃OH, while some features are blends of lines. After subtraction of a linear baseline, Gaussian profiles were fitted to extract line parameters. The free parameters in these fits were the line flux $\int T_{\text{mb}} dV$, the FWHM line width and the central velocity. The retrieved line fluxes and widths are listed in Table 1, while the central velocities are consistent with those found for C¹⁷O and C³⁴S in van der Tak et al. (2000).

For most sources, the line widths are also consistent with those found for C¹⁷O and C³⁴S. However, for the two lowest-luminosity sources, GL 7009S and IRAS 20126, the methanol lines are much broader than those of C¹⁷O and C³⁴S. The CH₃OH line profiles toward these sources (Fig. 2) suggest an origin in their molecular outflows, especially in GL 7009S. The methanol emission toward young low-mass stars such as L 1157 (Bachiller et al. 1995) and NGC 1333 IRAS 4A (Blake et al. 1995) is also dominated by their outflows. The other sources studied here possess outflows, but those do not seem to be important for the CH₃OH emission. As we will show below, the observed gas-phase CH₃OH is mostly due to evaporation of grain mantles. The CH₃OH line profiles thus suggest that around low-mass stars, the desorption of icy grain mantles is dominated by shocks, while radiative heating dominates for high-mass stars.

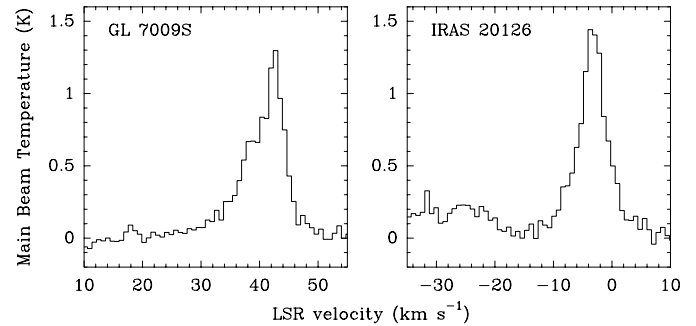


Fig. 2. Line profiles of CH₃OH $5_{-0} \rightarrow 4_{-0} \text{ A}^+$ toward GL 7009S and IRAS 20126. The outflow wing is most prominent in GL 7009S. The feature at -25 km s^{-1} in IRAS 20126 is the $K = 4$ A line.

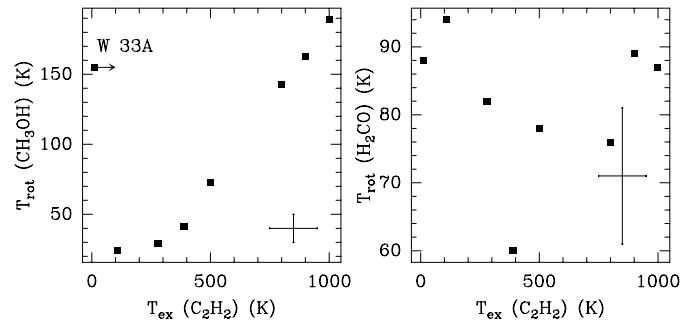


Fig. 3. Rotation temperatures of CH₃OH (*left*) and H₂CO (*right*) versus excitation temperatures of C₂H₂ measured in infrared absorption. Crosses in the bottom right denote typical error margins.

The sources exhibit clear variations in their methanol spectra, both in absolute line strength and in the relative strength between lines. Variations in absolute line strength can be due

to differences in molecular abundances, the size of the emitting region or distance, while the line ratios reflect differences in the temperature and density of the emitting gas. Before modeling the observations in detail, we perform a quick-look examination using rotation diagrams, as in Blake et al. (1987) and Helmich et al. (1994). This analysis assumes that the emission is optically thin and that the population of the molecular energy levels can be described by a single temperature, the “rotational temperature”. Since the envelopes of these stars are known to have temperature and density gradients, the rotation temperature gives information where the molecule is preferentially located in the envelope. The nondetection of ¹³CH₃OH lines limits the optical depth of the lines to $\lesssim 3$, except in the case of NGC 6334 IRS1, where the strongest lines are probably saturated.

Table 2 presents the results of the rotation diagram analysis, which are averages over the JCMT beam. Formal errors from the least-square fit to the data and calibration errors combine into uncertainties of 20% in both parameters. The results for IRAS 20126, W 3 (H₂O) and NGC 6334 IRS1 are more uncertain, to $\approx 50\%$, because the derived T_{rot} is close to the highest observed energy level. The OVRO maps presented in Sect. 3.2 indicate that the CH₃OH column densities are beam diluted by a factor of ~ 25 ; this information is not available for H₂CO. Although the column densities of the two species are roughly correlated, with $N(\text{CH}_3\text{OH}) \sim 10 \times N(\text{H}_2\text{CO})$, their excitation temperatures behave differently. While $T_{\text{rot}}(\text{H}_2\text{CO})$ is rather constant from source to source, 60–90 K, except toward the hot cores W 3 (H₂O) and NGC 6334 IRS1, the CH₃OH excitation temperatures span the full range 10–200 K.

The spectral line survey of Thompson & MacDonald (1999) toward W 28 A2 includes the CH₃OH $J = 7 \rightarrow 6$ band, and their analysis gives $T_{\text{rot}} = 49$ K and $N = 3.8 \times 10^{15} \text{ cm}^{-2}$, in good agreement with our results from the $J = 5 \rightarrow 4$ band. Our values of $N(\text{H}_2\text{CO})$ toward W 3 (H₂O) and NGC 6334 IRS1 are a factor of ~ 10 higher than those found by Mangum & Wootten (1993), probably due to the smaller JCMT beam size.

Fig. 3 compares the rotational temperatures of CH₃OH and H₂CO to the C₂H₂ excitation temperatures measured by Lahuis & van Dishoeck (2000) in absorption at 13.7 μm for the same lines of sight. Lacking a dipole moment, C₂H₂ is a clean probe of temperature. The tight correlation between the CH₃OH and C₂H₂ excitation temperatures implies that the two species trace the same gas, and that source orientation and optical depth effects do not influence the infrared data. The only exception is W 33A: this massive source becomes optically thick at 14 μm before the warm gas is reached. In contrast, the H₂CO temperature is not correlated with that of C₂H₂: omitting W 33A, the correlation coefficient is 7.8%, versus 98.3% for CH₃OH. This difference indicates that in these sources, H₂CO is not chemically related to CH₃OH and C₂H₂, unlike in low-mass objects, as the high H₂CO abundance in the L 1157 outflow (Bachiller & Pérez Gutiérrez 1997) and the detection of HDCO and D₂CO in IRAS 16293 (van Dishoeck et al. 1995; Ceccarelli et al. 1998) indicate.

3.2. Interferometric maps of CH₃OH line emission

Fig. 4 presents the OVRO observations, as maps of the emission integrated over the line profile. These maps were obtained by a gridding and fast Fourier transform of the (u, v) -data with natural weighting, and deconvolution with the CLEAN algorithm. The self-calibration solutions obtained for the continuum data were used to suppress phase noise introduced by the atmosphere. Also shown are spectra at the image maxima, extracted from image cubes at full spectral resolution and coverage. In these maps and spectra, the continuum emission has not been subtracted. Only in the case of NGC 7538 IRS1, the continuum brightness is comparable to the line brightness; for the other sources, the continuum can be neglected.

The maps show single, compact emitting sources, which coincide within the errors with their counterparts in 86–230 GHz continuum emission (van der Tak et al. 1999, 2000). No CH₃OH line emission was detected toward NGC 7538 IRS9 to the 1σ noise level of ≈ 1 K. In the case of W 33A, a binary source at these wavelengths, the CH₃OH emission is associated with the source MM1 from van der Tak et al. (2000) and with the infrared source. Although the CH₃OH emission is seen to be slightly extended toward the West, no emission was detected at the position of the other continuum source, MM2.

Table 3 lists various parameters of the lines observed with OVRO. Deconvolved source sizes were obtained by fitting two-dimensional Gaussian profiles to the integrated emission maps; other parameters by fitting Gaussians to the presented spectra. The continuum emission was subtracted from the data before this fitting procedure.

The measured central velocities and line widths are consistent with the values measured with the JCMT. To check if the two telescopes indeed trace the same gas, we have calculated the line strengths expected from the JCMT rotation diagrams. For the sources where CH₃OH is detected with OVRO, we predict a brightness of 15–30 K in the CH₃OH 107 GHz line and of 10–15 K in the 104 GHz line, in good agreement with the data. For NGC 7538 IRS9, which has a low CH₃OH rotation temperature, we expect $T_B \approx 60$ K in the 107 GHz line. The lack of CH₃OH emission in the OVRO data suggests that there is a gradient in T_{ex} from ≈ 30 K on a 15'' scale (traced by the JCMT but resolved out by OVRO) to ≈ 100 K within the 3'' OVRO synthesized beam. For the other sources, the bulk of the envelope may already be heated to ≈ 100 K and up.

3.3. Maser emission

While the $V_{\text{LSR}} = -53.9 \text{ km s}^{-1}$ component in the 107 GHz line profile observed toward NGC 7538 IRS1 with OVRO has a brightness and a width consistent with the JCMT data of this source, the brightness of the other velocity components is a factor of 2–5 higher than expected from the JCMT data. This difference suggests that the observed emission is amplified by a maser process. This possibility is supported by the line profile with three narrow velocity peaks (Fig. 4). Maser emission has been observed toward this source in several lower-frequency

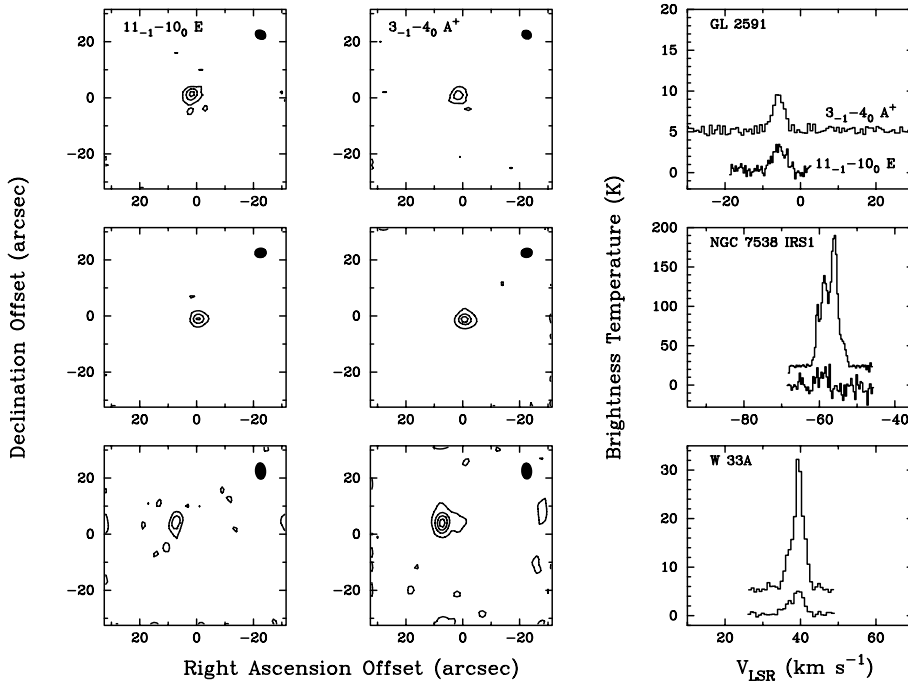


Fig. 4. Maps and spectra of CH₃OH line emission, made with the OVRO array. Contour levels for GL 2591 (top row) are: 60, 180, 300 mJy beam⁻¹ for both images; for NGC 7538 IRS1 (middle row): 300, 900, 1500 mJy beam⁻¹ (left) and 400, 2400 and 4400 mJy beam⁻¹ (right); and for W 33A (bottom row): 100, 200 mJy beam⁻¹ (left) and 100, 300, 500, 700 mJy beam⁻¹ (right). In the spectrum of NGC 7538 IRS1, the brightness of the 11₋₁ – 10₀ E line has been increased by a factor of 4.

methanol lines, by Wilson et al. (1984) and Batrla et al. (1987), at velocities consistent with the two strongest components reported here. Using VLBI, Minier et al. (1998) resolved the maser emission in the 5₁ → 6₀ A⁺ (6.67 GHz) and 2₀ → 3₋₁ E (12.2 GHz) lines into eleven spots, with sizes of < 10⁻³ arc seconds each. The spots at velocities -57 → -62 km s⁻¹ lie in an outflow, but the kinematics of the brightest masers, those at ≈ -56 km s⁻¹, are consistent with an origin in a disk. These two lines as well as the 107 GHz line are transitions to the *K*-ground state (so-called Class II masers), which require a strong continuum radiation field to be pumped (Cragg et al. 1992). In the case of NGC 7538 IRS1, this radiation is provided by the H II region, consistent with the fact that among the sources studied here with OVRO, only NGC 7538 IRS1 displays maser emission, which is also the source with the strongest H II region. For the 1₁₀ → 1₁₁ line of H₂CO, where Rots et al. (1981) observed maser action at similar velocities, the same pump mechanism operates, as demonstrated by Boland & de Jong (1981).

The brightness ratio of the 6.67 to 12.2 GHz methanol maser lines measured by Minier et al. (1998) is ≈ 10. Comparing this number with the models by Sobolev et al. (1997), we find $N(\text{CH}_3\text{OH}) \sim 10^{16}$ cm⁻². This value is similar to $N(\text{H}_2\text{CO})$ from Boland & de Jong (1981), which is a lower limit because Rots et al. (1981) did not resolve the emission spatially. The ratio $N(\text{H}_2\text{CO})/N(\text{CH}_3\text{OH})$ for the disk of NGC 7538 IRS1 is therefore $\gtrsim 1$, which is significantly larger than in the extended envelopes.

4. Abundance profiles of CH₃OH and H₂CO

In this section, we proceed to interpret the CH₃OH and H₂CO observations in terms of the detailed physical models developed

by van der Tak et al. (2000). These models use a power law density structure, $n = n_0(r/r_0)^{-\alpha}$. Specific values for the density gradient α , the size scale r_0 and the density scale n_0 for every source can be found in van der Tak et al. (2000). These values, as well as temperature profiles, have been derived from dust continuum and CS, C³⁴S and C¹⁷O line observations at submillimeter wavelengths.

4.1. Constant-abundance models

Using the density and temperature profiles, we have first attempted to model the data using constant abundances of H₂CO and CH₃OH throughout the envelopes. This assumption is motivated by the fact that in models of pure gas-phase chemistry, the abundances of H₂CO and CH₃OH do not change much in the range 20–100 K. Molecular excitation and radiative transfer are solved simultaneously with a computer program based on the Monte Carlo method, written by Hogerheijde & van der Tak (2000). The emission in all observed lines is calculated, integrated over velocity, and convolved to the appropriate telescope beam. Comparison to observations proceeds with the χ^2 statistic described in van der Tak et al. (2000).

The collisional rate coefficients for CH₃OH have been provided by M. Walmsley (1999, priv. comm.), and are based on the experiments by Lees & Haque (1974). A detailed description of the coefficients is given by Turner (1998). Following Johnston et al. (1992), we have set the $\Delta K = 3$ rates to 10% of the $\Delta K = 1$ values.

The results of the model calculations are shown in Fig. 5, and the derived best-fit abundances are given in Column 6 of Table 2. In the figure, the observed and modeled line fluxes have been

Table 3. Parameters of line emission observed with OVRO

Source	Line	LSR Velocity km s ⁻¹	ΔV (FWHM) km s ⁻¹	Peak T_B K	Source Size arcsec	Beam Size arcsec
GL 2591	3 ₁ → 4 ₀ A ⁺	-5.8	3.5	4.3	3.4 × 2.7	3.4 × 2.9
	11 ₋₁ → 10 ₋₂ E	-5.7	4.0	2.8	3.1 × 2.3	3.8 × 3.0
W 33A	3 ₁ → 4 ₀ A ⁺	39.5	3.5	23.3	3.9 × 3.0	5.6 × 3.4
	11 ₋₁ → 10 ₋₂ E	39.1	4.3	4.4	6.4 × 2.2	5.7 × 3.5
NGC 7538 IRS1	3 ₁ → 4 ₀ A ⁺	-60.5	1.4	63.6	–	3.9 × 3.2
		-58.6	1.8	108.	–	3.9 × 3.2
		-56.1	1.9	164.	–	3.9 × 3.2
		-53.9	2.5	29.2	–	3.9 × 3.2
	11 ₋₁ → 10 ₋₂ E	-59.0	2.8	4.2	1.8 × 0.7	4.0 × 3.3

converted to column densities following Helmich et al. (1994). Three types of sources can be distinguished. Most sources can be fitted with CH₃OH/H₂ ∼ 10⁻⁹, similar to the values found for dark and translucent clouds (Turner 1998; Takakuwa et al. 1998), while the “hot core”-type sources W 3(H₂O), NGC 6334 IRS1 and W 28 A2 require abundances of a few times 10⁻⁸. However, for three sources, no single methanol abundance gives a good fit.

4.2. Jump models

For the sources W 33A, GL 2591 and NGC 7538 IRS1, the lines from energy levels $\gtrsim 100$ K above ground require significantly higher abundances than the lower-excitation lines. These results suggest that the abundance of CH₃OH is higher in the warm, dense gas close to the star than in the more extended, cold and tenuous gas. From the location of the break in the abundance profile, it seems likely that evaporation of grain mantles, which also occurs at ~ 100 K, plays a role. As a simple test of ice evaporation, we have run models for these three sources where the CH₃OH abundance follows a step function. In these “jump” models, the CH₃OH abundance is at a low level, the “base level”, far from the star, while at a threshold temperature, the abundance surges to a high value, the “top level”. The situation is sketched in Fig. 6. The motivation for this model is that if methanol is present in icy grain mantles, its abundance will increase strongly when these ices evaporate. For the temperature threshold, we take 90 K, which is where water ice, the most refractory and most abundant component of the grain mantles, evaporates in ~ 10 yr (Sandford & Allamandola 1993).

Alternatively, the ice may be desorbed in a weak shock associated with the molecular outflows these sources are known to have: Jones et al. (1996) calculate that a local grain-grain velocity dispersion of ≈ 2 km s⁻¹ is sufficient to shatter ice material. Shock desorption of methanol is known to be important in low-mass protostars, for example L 1157 (Bachiller et al. 1995) and NGC 1333 IRAS 4A (Blake et al. 1995). The large line widths and line profiles measured here for the low-luminosity sources GL 7009S and IRAS 20126 indicate that shock desorption plays a role there; for the other sources, thermal effects probably dominate. Since CH₃OH is confined to the refractory (polar) component of the ice, it is not necessary to consider the

effect of a slowly rising temperature in the hot core region, as Viti & Williams (1999) did.

For the base level, we take the abundances found in the previous section, which were constrained mostly by the low- K lines with $E < 100$ K. We have considered jump factors of 3, 10, 30, 100 and 300 without further iteration. Between these models, jumps by factors of ~ 30 give the best match to the high-excitation lines. The results of these models are plotted as squares in Fig. 5 and listed in Column 6 of Table 2.

Further constraints on the abundance profile of CH₃OH in our sources may be obtained by comparing the models to the OVRO data. The points in Fig. 7 are the OVRO visibility data of W 33A and GL 2591. The observations of the 107 GHz line have been integrated over velocity and binned in annuli around the source position. Superposed are model points for the constant-abundance model and for the jump model. The data do not particularly favour one model or the other, perhaps because this transition traces mostly cold gas. Collisional rate coefficients up to $J = 11$ are eagerly awaited, so that the 104 GHz line can be modeled as well.

5. Discussion

5.1. Relation to solid-state observations

The enhancement of the methanol abundance at high temperatures is very likely related to the evaporation of solid methanol, which has been observed at infrared wavelengths toward many of the sources studied here (Sect. 1). Ground-based data already revealed that CH₃OH is not mixed with the bulk of the water ice (Skinner et al. 1992). Recent ISO results indicate extensive ice segregation toward massive young stars; the absorption profiles of CO₂ ice indicate that the methanol resides in a H₂O:CH₃OH:CO₂=1:1:1 layer heated to ≈ 80 K as shown by Ehrenfreund et al. (1998), Gerakines et al. (1999) and Dartois et al. (1999a). The column density of solid CH₃OH is typically $\sim 5\%$ of that of water ice, but in two cases, W 33A and GL 7009S, it is as high as 30%. It has been suggested that CH₃OH ice is preferentially formed around more massive young stars, but among the sources studied here, these two do not stand out in luminosity. Instead, they are the two most embedded sources in the sample (see van der Tak et al. 2000), which may enhance the formation of solid methanol. The gas-phase

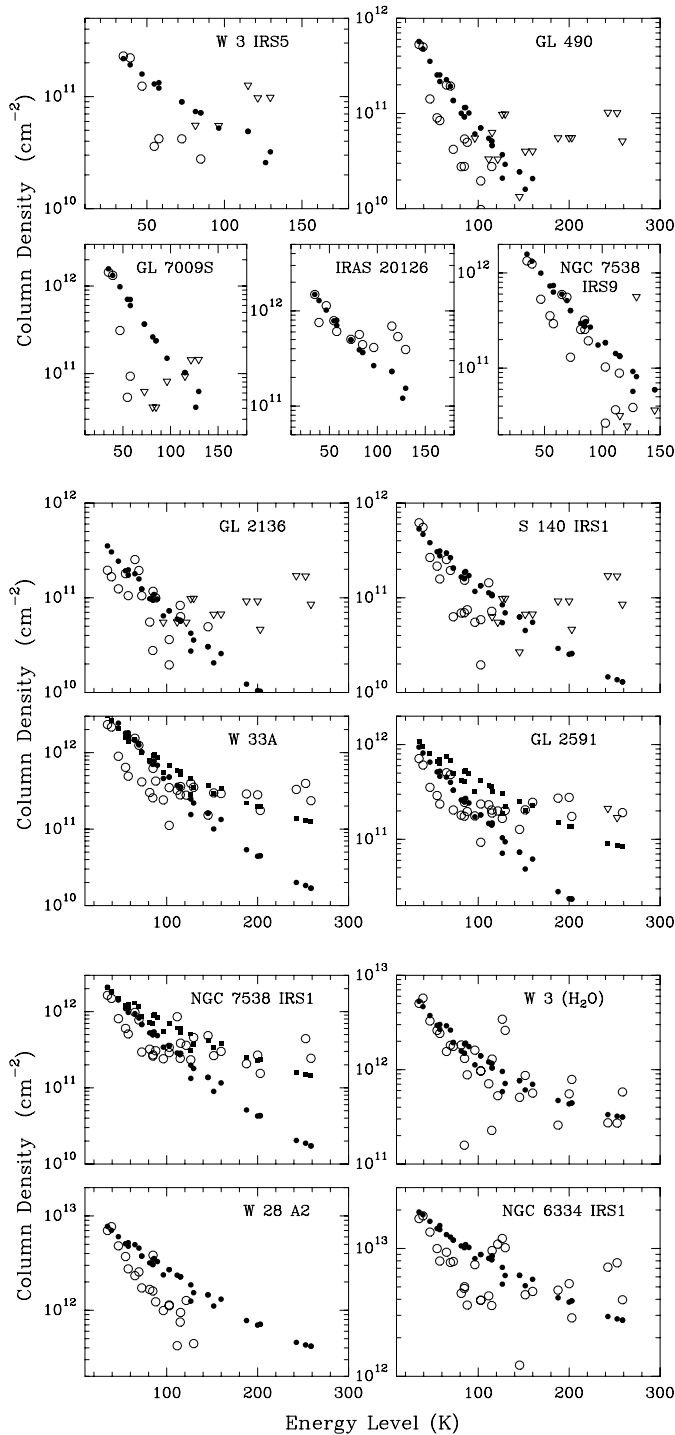


Fig. 5. Results of Monte Carlo models for CH₃OH, with ‘cold’ sources at the top, ‘jump’ sources in the middle and ‘hot cores’ at the bottom. Filled symbols are line strengths predicted by the best-fit constant-abundance models (circles) and jump models (squares) for W 33A, GL 2591 and NGC 7538 IRS1. Open symbols are JCMT data, with circles indicating detections and triangles upper limits. The data on W 28 A2 include those of Thompson & Macdonald 1999.

abundance of CH₃OH (Table 2) is much lower in GL 7009S than that in W 33A, suggesting that GL 7009S is in an earlier evolutionary state where ice evaporation affects only a small part of the envelope.

A link between solid and gaseous methanol is plausible because the sources with high gas-phase CH₃OH abundances are also the ones with high fractions of annealed solid ¹³CO₂ (Boogert et al. 2000), and high abundances of gas-phase H₂O and CO₂ (Boonman et al. 2000). These molecules evaporate at ~ 90 K, like methanol. The CH₃OH abundances also follow the ratios of envelope mass to stellar mass and the 45/100 μ m colours from van der Tak et al. (2000), which confirms the picture that warmer sources have higher molecular abundances in the gas phase. These results indicate that the excitation and abundance of gaseous CH₃OH can be used as evolutionary indicators during the embedded stage of massive star formation. As discussed in Sect. 3.1, using submillimeter data to trace evolution has the advantage of being independent of source orientation or total mass, because the dust emission is optically thin at these wavelengths.

Grain mantle evaporation appears to be much less important for H₂CO than for CH₃OH. We have compared the H₂CO data to the constant-abundance models from van der Tak et al. (2000) in similar plots as Fig. 5, and found good agreement. There is no evidence for jumps in the H₂CO abundance by factors $\gtrsim 3$ within the temperature range of 20–250 K that the observations are sensitive to. This result suggests that the formaldehyde observed in these sources is predominantly formed in the gas phase by oxidation of CH₃. Gas-phase models by Lee et al. (1996) indicate an abundance of $\sim 10^{-9}$, similar to the observed value, although a contribution from ice evaporation at the 10^{-9} level cannot be excluded.

The high observed HDCO/H₂CO ratios and the detections of D₂CO toward the Compact Ridge in Orion (Wright et al. 1996; Turner 1990) and toward embedded low-mass objects such as IRAS 16293 (van Dishoeck et al. 1995; Ceccarelli et al. 1998) indicate H₂CO formation on grains. In our sources, HDCO is not detected to H₂CO/HDCO > 10; in a survey of hot core-type sources, Hatchell et al. (1998) obtained DCN/HCN $\sim 10^{-3}$, much lower than in embedded low-mass stars. Although the surface chemistry should qualitatively be the same, the cold (~ 10 K) phase may last too short in our sources to build up large amounts of deuterated molecules such as those seen in the Compact Ridge and in low-mass objects.

In eleven regions of (mostly massive) star formation, Mangum & Wootten (1993) derived ratios of ortho- to para-H₂CO of 1.5–3 and took this result as evidence for grain surface formation of H₂CO. However, this conclusion appears tentative, since for most of their sources, only one line of ortho-H₂CO was observed. In addition, at the H₂CO column densities of $\sim 10^{14}$ cm⁻², representative of the regions studied by Mangum & Wootten and by us, the $K = 0$ and $K = 1$ lines of H₂CO have optical depths of ~ 1 , requiring careful modeling. The data and models presented in this paper are consistent with an ortho-/para-H₂CO ratio of 3.

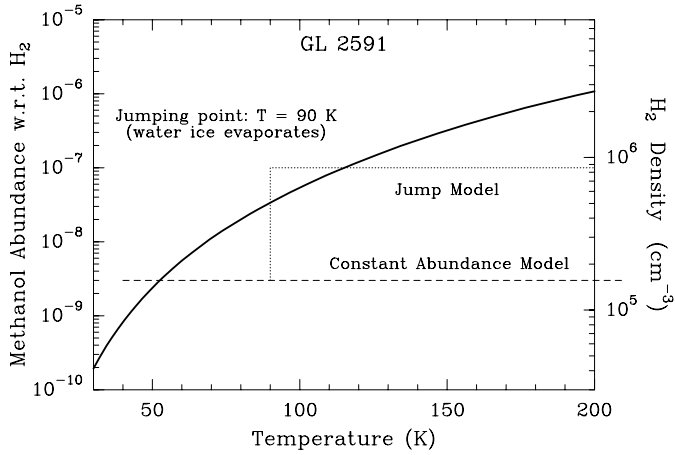


Fig. 6. Density and temperature structure (solid line) and abundance profiles (dotted and dashed lines) of the two models for CH₃OH in the source GL 2591.

High abundances of methanol as observed in the ices, $\sim 10^{-6}$ relative to hydrogen, cannot be produced in the gas phase, except maybe in shocks. This mechanism has been proposed for H₂O ice by Bergin et al. (1999) and for CO₂ by Charnley & Kaufman (2000); its application to CH₃OH depends on the existence of a high-temperature route to form methanol, which is not yet known. Hartquist et al. (1995) proposed the reaction CH₄+OH, but ISO-SWS observations by Boogert et al. (1998) indicate low abundances of gaseous methane in our sources, and at $T \gtrsim 200$ K, all OH should be consumed by H and H₂ to form H₂O. The widths of the CH₃OH lines of only a few km s⁻¹ also argue against formation in shocks.

More likely, the solid methanol is formed by reactions on or inside the ice layers. Addition of H atoms to CO molecules will lead to H₂CO, and further to CH₃OH. In the literature, there are three proposed sources of atoms: direct accretion from the gas phase, ultraviolet irradiation and bombardment by energetic particles. We show in Sect. 5.4 that the latter two mechanisms are unlikely to be important for the sources studied in this paper, and focus for now on the first.

5.2. Surface chemistry model

If the CH₃OH ice that we see evaporating in these sources originates from H atom addition (=reduction) of CO ice on the surfaces of dust grains, it cannot have been produced under the current physical conditions. The evaporation temperature of CH₃OH and H₂O ice, 90 K, is much higher than that of CO and O, ≈ 20 K, and that of H, ≈ 10 –15 K, depending on its surface mobility and reactivity. Any formation of CH₃OH ice through surface reduction of CO must therefore have occurred before the central star heated up its envelope above ~ 15 K. The most likely phase of the cloud to form methanol ice through surface chemistry is therefore the pre-protostellar phase, when the grain temperature may have been as low as ≈ 10 K and the cloud was contracting to form a dense core. However, about 1/3 of solid CO

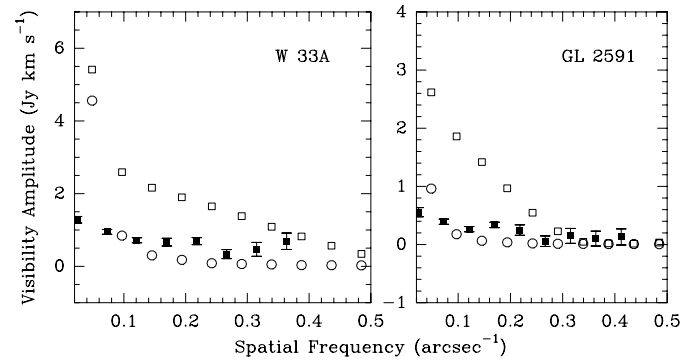


Fig. 7. Visibility amplitudes of CH₃OH 3₁ → 4₀ A⁺ emission as observed with OVRO toward W 33A (left) and GL 2591 (right), and model points for the constant-abundance (open circles) and the “jump” models (open squares).

is observed inside the water ice layer, and will not evaporate until much higher temperatures are reached (Tielens et al. 1991). If H and O atoms can be similarly trapped, solid-state reduction and oxidation may occur at temperatures well above 20 K.

Tielens & Hagen (1982) and Tielens & Allamandola (1987) proposed that direct accretion of atoms and molecules from the gas phase, followed by low-temperature surface reactions, determine the composition of grain mantles. Activation barriers are offset by the long effective duration of the collision on the surface. The resulting mantle composition is determined by the relative accretion rates of H and CO onto the grains, and the relative height of the reaction barriers.

This mechanism predicts that the abundance ratios of H₂CO/CH₃OH and CO/CH₃OH are correlated, as shown by the curve in Fig. 8, taken from Charnley et al. (1997), with the reaction probability ratio ϕ_{H} of CO + H to H₂CO + H is 10^{-3} . Along the curve, the H/CO abundance ratio decreases down to 10^{-2} at its tip. At the density in the central regions of our sources, $\sim 10^6$ cm⁻³, atomic H is mainly produced by cosmic-ray ionization of H₂, giving a constant concentration of ~ 1 cm⁻³, or an abundance of 10^{-6} . The abundance of CO in these sources was measured by van der Tak et al. (2000) to be $\approx 1 \times 10^{-4}$, as expected if all gas-phase carbon is in CO and no significant depletion occurs. Hence, H/CO $\approx 10^{-2}$, and our sources should lie right at the tip of the curve. The value $\phi_{\text{H}} = 10^{-3}$ implies that the CO → H₂CO reaction limits the rate of CH₃OH formation, consistent with the non-detection of evaporated H₂CO.

The figure also plots the observed abundance ratios, where the H₂CO and CO abundances have been taken from van der Tak et al. (2000), while for CH₃OH, either the constant-abundance model or the “top level” of the jump model has been plotted. The data points are seen to lie along a “sequence” which lies along the model curve, perhaps displaced toward lower CH₃OH abundances by an order of magnitude. Although this behaviour is consistent with solid-state formation of H₂CO and CH₃OH at various H/CO ratios, the different rotation temperatures and abundance profiles of H₂CO and CH₃OH argue against a common chemical origin for these two species, and favour complete hydrogenation of CO into CH₃OH. The figure

also plots solid state observations by Keane et al. (2000), which are lower limits in the case of CO because of evaporation.

Since the abundances of CO and H₂CO are almost the same in all our sources, the spread in the abundance ratios is probably due to different degrees of CH₃OH evaporation and subsequent gas-phase destruction. Indeed, the abundances of gaseous CH₃OH are factors of $\gtrsim 10$ lower than the values measured in the solid state. This difference is expected since methanol is destroyed in $\sim 10^4$ yr (Charnley et al. 1992) in reactions with ions such as H₃⁺, leading to a rich chemistry with species like CH₃OCH₃ and CH₃OCHO. These species are indeed detected toward the “hot cores” W 3 (H₂O) and NGC 6334 IRS1, weaker toward the “jump sources” GL 2591 and NGC 7538 IRS1, and absent in the low-methanol source W 3 IRS5 (Helmich & van Dishoeck 1997; van Dishoeck & van der Tak 2000).

We conclude that the observed spread in the gaseous methanol abundance is due to incomplete evaporation for the cold sources, which are the least evolved ones in our sample, and to gas-phase reactions for the hot cores, which are the most evolved. The most likely source of the methanol is grain surface chemistry in the pre-protostellar phase. The conditions in this phase cannot be derived by comparison to CO and H₂CO, for which our data suggest that gas-phase processes control the chemistry. A more promising molecule is CO₂.

5.3. The H/O competition:

density and duration of the pre-stellar phase

The ISO detection of ubiquitous solid CO₂ by Gerakines et al. (1999) makes clear that oxidation of CO is a potentially important competitor to reduction. These data are shown in the bottom panel of Fig. 8, as well as gas-phase CO₂ abundances from Boonman et al. (2000). Gas-grain chemistry is clearly important for CO₂, as it is for CH₃OH, warranting a comparative study of the two. The model by Charnley et al. (1997) did not include reactions with O, while Tielens & Hagen (1982) used O₂ as the dominant form of oxygen, which is inconsistent with recent observational limits (Melnick 2000). We have constructed a model of gas-grain chemistry based on the modified rate equation approach described in Caselli et al. (1998), and extensively tested against a Monte Carlo program. The chemical system consists of three gaseous species: H, O and CO, and eight surface species: OH, H₂O, O₂, CO₂, HCO, H₂CO, CH₂OH and CH₃OH. The calculations assume fast quantum tunneling of hydrogen, as proposed by Tielens & Hagen (1982). If hydrogen does not tunnel, as measurements by Katz et al. (1999) suggest, our simple system is unable to form significant mole fractions of CH₃OH and CO₂. In the case of reduced mobility for all species, the Eley-Rideal mechanism should be considered to model surface chemistry (Herbst 2000), which is not included here.

The mantle composition (Table 4) depends on density through the composition of the gas phase, in particular the H/O ratio. We take the concentrations of H, O and CO from Lee et al. (1996), for the case of low metals, $T = 10$ K,

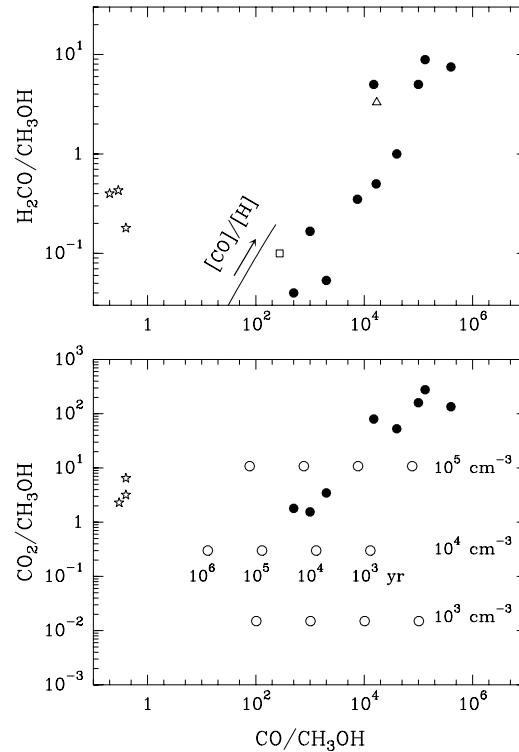


Fig. 8. Filled circles: observed abundance ratios of H₂CO/CH₃OH (top) and CO₂/CH₃OH (bottom) versus that of CO/CH₃OH. Open triangle: data on translucent clouds from Turner (1998); open square: data on the compact ridge in Orion from Sutton et al. (1995). Stars: solid-state data from Keane et al. (2000). Heavy line: surface chemistry model after Charnley et al. (1997). Open circles: results of surface chemistry model, labeled by time and density of the gas phase.

in steady state. The main result is that after reduction to HCO, CO is mostly reduced into CH₃OH at low densities and mostly oxidized at higher densities. In our model, the reaction CO+O→CO₂ has a barrier of 1000 K (see d’Hendecourt et al. 1985), else ices of 60% CO₂ would form which are not observed. Water is copiously made through the sequence O+H→OH and OH+H→H₂O. The detailed composition of the grain mantles is quite uncertain because of unknown reaction rates. For instance, the fraction of H₂CO depends on relative barrier height of the CO+H and H₂CO+H reactions, but H₂CO is never a major component of the ice layer, consistent with gas-phase and solid state observations. The results in Table 4 refer to a chemical time scale of 1000 years. Unlike inert species such as O₂, H₂O, CH₃OH and CO₂, the fractions of trace species (fractions $\lesssim 0.01$) also depend somewhat on time, and are not used in the analysis. Species that react quickly with H maintain a constant population because they are hydrogenated on the H accretion time scale (~ 1 day if $n_{\text{H}} = 10^3$ cm⁻³), and their molar fractions decline as the ice layer grows with time.

As an example, we will now estimate the yield of CH₃OH by this scheme for the case $n_{\text{H}} = 10^4$ cm⁻³. The depletion rate of CO molecules from the gas phase is $f_d = n_d \sigma V_{\text{CO}} S$, with n_d and σ the number density and cross section of the dust grains, V_{CO} the thermal velocity of CO and S the sticking coefficient,

Table 4. Results of gas-grain chemical model at $T = 10$ K.

Species	Total density n_{H}		
	10^3	10^4	10^5
Gas phase concentrations (cm^{-3})			
H	1.15	1.15	1.1
O	0.09	0.75	7.0
CO	0.075	0.75	7.5
Molar fractions in the solid state			
O ₂	9.3(-3)	0.11	0.27
H ₂ O	0.60	0.37	0.12
H ₂	0.0	0.0	0.0
CO	1.4(-5)	3.9(-5)	0.48
H ₂ CO	1.4(-5)	3.1(-5)	3.1(-2)
CH ₃ OH	0.39	0.41	7.8(-3)
CO ₂	6.1(-3)	0.12	8.7(-2)

assumed to be 10%. Taking silicate grains of radius $0.1 \mu\text{m}$, $f_d = 3 \times 10^{-15} \text{ s}^{-1}$, or 10% in 10^6 years. At this density, 77% of this depleted CO goes into CH₃OH, so that upon evaporation, the abundance ratio would be $\text{CH}_3\text{OH}/\text{CO} \approx 0.086$ or $\text{CH}_3\text{OH}/\text{H}_2 \sim 10^{-5}$.

Assuming that the composition of ice layers is determined by surface chemistry, our model can be used to investigate the initial conditions of massive star formation by considering abundance ratios of CO, CO₂ and CH₃OH. The CO₂/CH₃OH ratio is sensitive to density, independent of time, and equals the ratio of the molar fractions of solid CO₂ and CH₃OH in Table 4. Time is measured by the ratio of raw material (CO) to product (CH₃OH) through the fraction of CO in the solid state derived above, $0.01(t/10^5 \text{ yr})(n_{\text{H}}/10^4 \text{ cm}^{-3})$. The abundance ratio in the gas phase is this fraction multiplied by the efficiency of CO→CH₃OH conversion, equal to the molar fraction of CH₃OH divided by the sum of the fractions of CO and its possible products, CO₂, H₂CO and CH₃OH. Fig. 8 plots the synthetic abundance ratios as open circles, labeled by time and density. If this model is valid, the observed CO₂/CH₃OH ratio constrains the density in the pre-protostellar phase to be $\approx 10^5 \text{ cm}^{-3}$, or higher, since some CO₂ may be destroyed shortly after evaporation. At this density, hydrogenation of CO is incomplete due to the low H flux, and a significant abundance of solid H₂CO is expected, consistent with the results of Keane et al. (2000). Using this limit on the density, the observed CO/CH₃OH ratio constrains the time spent in the pre-protostellar phase to be $\lesssim 10^5$ years within the grain surface chemistry scenario. The same conclusion is reached when the CO/CO₂ ratio is used instead of CO/CH₃OH; the uncertainty is a factor of ten due to the unknown sticking coefficient. This time scale is significantly smaller than the corresponding number for low-mass stars, where this phase lasts $\sim 10^6$ years as derived from the ratio of dense cores with and without stars found by Beichman et al. (1986). The same time scale of $\sim 10^6$ yr is obtained from our models for an abundance ratio of CO/CH₃OH $\sim 10^3$, as observed in the compact ridge in Orion.

These models also help to understand observations of solid CO₂ in other regions where no star formation is occurring. Toward the field star Elias 16 behind the Taurus dark cloud, CO₂ has been detected (Whittet et al. 1998) but CH₃OH has not (Chiar et al. 1996). The models suggest thus that the density in this region is $\gtrsim 3 \times 10^4 \text{ cm}^{-3}$. The model does not explain the lack of solid CH₃OH toward SgrA* ($\lesssim 3\%$ relative to H₂O ice; Chiar et al. 2000), where CO₂ ice has been detected. For this low-density line of sight, the opposite ratio would be expected. An enhanced temperature or ultraviolet irradiation may be important here. For the disk around NGC 7538 IRS1, where $N(\text{H}_2\text{CO})/N(\text{CH}_3\text{OH}) \gtrsim 1$ (Sect. 3.3), the models indicate that the density is $\gtrsim 10^5 \text{ cm}^{-3}$.

The model is also consistent with current observational limits on solid O₂. At low densities, our models drive all O into H₂O on the dust grains, but for $\geq 10^5 \text{ cm}^{-3}$, part of it goes into O₂. However, the ratio O₂/CO remains < 1 on the surface, in agreement with the limit derived by Vandenbussche et al. (1999) from ISO-SWS observations of NGC 7538 IRS9. Evaporation of solid O₂ plays a role, but observations of gaseous O₂ with the Submillimeter Wave Astronomy Satellite give an upper limit toward massive star-forming regions of $\sim 10^{-7}$ relative to H₂ (Melnick 2000), consistent with the solid-state results.

5.4. Alternative models

Could ultraviolet irradiation or energetic particle bombardment also produce the observed trends in the abundances? The production rate of species i by irradiation can be written as $dn_i/dt = \alpha_i \Phi 4\pi r_g^2$, with Φ the ultraviolet flux in photons $\text{cm}^{-2} \text{ s}^{-1}$ and r_g the radius of the dust grains, taken to be 10^{-5} cm . Inside dense clouds, most ultraviolet radiation is produced by cosmic-ray interaction with H₂, which gives a field approximately equal to the interstellar radiation field at $A_V = 5$ (Prasad & Tarafdar 1983), or 5000 photons $\text{cm}^{-2} \text{ s}^{-1}$. The reaction yields α_i follow from laboratory experiments such as those reported at the Leiden Observatory Laboratory database³, in this case on a mixture of initial composition H₂O:CO = 100:33. The amounts of CH₃OH and CO₂ produced do not depend on this ratio as long as it is > 1 . Using band strengths by Gerakines et al. (1996) and Kerkhof et al. (1999), we obtain $\alpha = 1.9 \times 10^{-3}$ for CH₃OH and $\alpha = 3.2 \times 10^{-2}$ for CO₂. The ratio of these numbers is in good agreement with the observed abundance ratio of ~ 10 . However, the absolute values of the α_i imply production rates of $\sim 10^{-8} \text{ s}^{-1}$ per grain, compared to the accretion rate of H, O and CO of $\sim 10^{-5} \text{ s}^{-1}$. Stellar ultraviolet radiation can only affect the inner parts of the envelopes since their extinctions are $A_V \sim 100$ magnitudes. The absence of a strong ultraviolet field throughout the envelopes of our sources is also suggested by the observational limits from ISO-SWS on mid-infrared fine structure lines and of emission by polycyclic aromatic hydrocarbons (van Dishoeck & van der Tak 2000).

The processing of interstellar ice by cosmic rays was studied by Hudson & Moore (1999), who bombarded an H₂O:CO=5:1

³ see www.strw.leidenuniv.nl/~lab

ice mixture with protons of energy ≈ 0.8 MeV. These experiments produced abundance ratios of H₂CO/CH₃OH=0.6 and CO₂/CH₃OH=2.0, in fair agreement with the observed values. Other species formed as well, notably formic acid (HCOOH) and methane (CH₄), which indeed are observed in interstellar grain mantles. However, the experiments by Hudson & Moore produced almost twice as much HCOOH and CH₄ as CO₂, while the observed abundances are only $\approx 10\%$ of that of CO₂ (Schutte et al. 1999; Boogert et al. 1998). In addition, the particle dose in the experiments was 2×10^{15} cm⁻², while the interstellar cosmic-ray flux is only 3 cm⁻² s⁻¹. Hence, the experiments simulate a bombardment for $\sim 3 \times 10^7$ yr, a factor of ~ 1000 longer than the ages of the sources studied here. Stellar X-ray emission (Glassgold et al. 2000) only acts on small scales, especially because of heavy attenuation in the envelopes of these obscured objects.

6. Conclusions

The chemistry of CH₃OH and H₂CO in thirteen regions of massive star formation is studied through single-dish (JCMT) and interferometer (OVRO) line observations at submillimeter wavelengths. Our main conclusions are:

1. The submillimeter emission lines of CH₃OH toward most sources have widths of 3–5 km s⁻¹, consistent with those found earlier for C¹⁷O and C³⁴S. However, in the low-luminosity sources GL 7009S and IRAS 20126, the line shapes reveal that CH₃OH is present in the outflow. These results indicate that the desorption of ices in the envelopes of low-mass protostars is primarily by shocks, while thermal processes dominate in the case of massive stars.
2. Rotational temperatures of CH₃OH range from 10 to 200 K and correlate very well with the excitation temperature of C₂H₂ measured in infrared absorption. This correlation suggests that both species trace the same gas, which may be outgassing of icy grain mantles. For H₂CO, the range in T_{rot} is only 60–90 K without relation to $T_{\text{ex}}(\text{C}_2\text{H}_2)$, suggesting a different chemical origin. We propose that $T_{\text{rot}}(\text{CH}_3\text{OH})$ can be used as evolutionary indicator during the embedded phase of massive star formation, independent of source optical depth or orientation.
3. Detailed non-LTE radiative transfer models of the CH₃OH lines suggest a distinction of three types of sources: those with CH₃OH/H₂ $\sim 10^{-9}$, those with CH₃OH/H₂ $\sim 10^{-7}$ and those which require a jump in its abundance from $\sim 10^{-9}$ to $\sim 10^{-7}$. The models are consistent with the $\approx 3''$ size of the CH₃OH 107 GHz emission measured interferometrically. The location of the jump at $T \approx 100$ K strongly suggests that the methanol enhancement is due to evaporation of icy grain mantles. The sequence of low-methanol \rightarrow jump \rightarrow high-methanol sources corresponds to a progression in the ratio of envelope mass to stellar mass and the mean temperature of the envelope. In contrast, the observed H₂CO seems primarily produced in the gas phase, since the H₂CO data can be well fit with a constant abundance of a few $\times 10^{-9}$ throughout the envelope. The grain surface hydrogenation of CO thus appears to be completed into CH₃OH, with little H₂CO left over.
4. Model calculations of gas-grain chemistry show that CO is primarily reduced (into CH₃OH) at densities $n_{\text{H}} \lesssim 10^4$ cm⁻³, and primarily oxidized (into CO₂) at higher densities. To keep sufficient CO on the grains, this mechanism requires temperatures of $\lesssim 15$ K, i.e., conditions before star formation. Assuming that surface reactions proceed at the accretion rate of CO, the observed CO₂ and CH₃OH abundances constrain the density in the pre-protostellar phase to be $n_{\text{H}} \gtrsim$ a few 10^4 cm⁻³, and the time spent in this phase to be $\lesssim 10^5$ yr. Our surface chemistry model predicts that lines of sight through clouds with a high H/O ratio will show abundant solid methanol and less CO₂. Ultraviolet photolysis and radiolysis by energetic (MeV) protons appear less efficient as ice processing mechanisms for these sources; radiolysis also overproduces HCOOH and CH₄.

Acknowledgements. The authors wish to thank Malcolm Walmsley for providing collisional rate coefficients for methanol, Xander Tielens, Pascale Ehrenfreund and Willem Schutte for comments on the manuscript and Ted Bergin, Eric Herbst, Friedrich Wyrowski and Wilfried Boland for useful discussions. Annemieke Boonman and Jacque Keane kindly provided us with their results in advance of publication. We are grateful to Remo Tilanus and Fred Baas at the JCMT and Geoffrey Blake at OVRO for assistance with the observations. This research was supported by NWO grant 614-41-003 and the MURST program “Dust and Molecules in Astrophysical Environments”.

References

- Allamandola L.J., Sandford S.A., Tielens A.G.G.M., Herbst T.M., 1992, ApJ 399, 134
- Bachiller R., Liechti S., Walmsley C.M., Colomer F., 1995, A&A 295, L51
- Bachiller R., Pérez Gutiérrez M., 1997, ApJ 487, L93
- Batrla W., Matthews H.E., Menten K.M., Walmsley C.M., 1987, Nat 326, 49
- Beichman C.A., Myers P.C., Emerson J.P., et al., 1986, ApJ 307, 337
- Bergin E.A., Neufeld D.A., Melnick G.J., 1999, ApJ 510, L145
- Blake G.A., Sandell G., van Dishoeck E.F., et al., 1995, ApJ 441, 689
- Blake G.A., Sutton E.C., Masson C.R., Phillips T.G., 1987, ApJ 315, 621
- Boland W., de Jong T., 1981, A&A 98, 149
- Boogert A.C.A., Helmich F.P., van Dishoeck E.F., et al., 1998, A&A 336, 352
- Boogert A.C.A., Ehrenfreund P., Gerakines P.A., et al. 2000, A&A 353, 349
- Boonman A.M.S., van Dishoeck E.F., Lahuis F., Wright C.M., Doty S.D., 2000, In: ISO beyond the peaks: The 2nd ISO workshop on analytical spectroscopy (ESA-SP), in press
- Caselli P., Hasegawa T.I., Herbst E., 1993, ApJ 408, 548
- Caselli P., Hasegawa T.I., Herbst E. 1998, ApJ 495, 309
- Ceccarelli C., Castets A., Loinard L., Caux E., Tielens A.G.G.M., 1998, A&A 338, L43
- Charnley S.B., Kaufman M.J., 2000, ApJ 529, L111
- Charnley S.B., Tielens A.G.G.M., Millar T.J., 1992, ApJ 399, L71
- Charnley S.B., Tielens A.G.G.M., Rodgers S.D., 1997, ApJ 482, L203
- Chiar J.E., Adamson A.J., Whittet D.C.B., 1996, ApJ 472, 665
- Chiar J.E., Tielens A.G.G.M., Whittet D.C.B., et al., 2000, ApJ 537, 749
- Cragg D.M., Johns K.P., Godfrey P.D., Brown R.D., 1992, MNRAS 259, 203

- Dartois E., Demyk K., d'Hendecourt L., Ehrenfreund P., 1999a, *A&A* 351, 1066
- Dartois E., Schutte W., Geballe T.R., et al., 1999b, *A&A* 342, L32
- d'Hendecourt L.B., Allamandola L.J., Greenberg J.M., 1985, *A&A* 152, 130
- Ehrenfreund P., Dartois E., Demyk K., d'Hendecourt L., 1998, *A&A* 339, L17
- Gerakines P.A., Schutte W.A., Ehrenfreund P., 1996, *A&A* 312, 289
- Gerakines P.A., Whittet D.C.B., Ehrenfreund P., et al., 1999, *ApJ* 522, 357
- Glassgold A.E., Feigelson E.D., Montmerle T., 2000, In: Mannings V.G., Boss A., Russell S.S. (eds.) *Protostars and Planets IV*, U. Arizona Press, p. 429
- Grim R.J.A., Baas F., Greenberg J.M., Geballe T.R., Schutte W., 1991, *A&A* 243, 473
- Hartquist T.W., Menten K.M., Lepp S., Dalgarno A., 1995, *MNRAS* 272, 184
- Hatchell J., Millar T.J., Rodgers S.D., 1998, *A&A* 332, 695
- Helmich F.P., Jansen D.J., de Graauw T., Groesbeck T.D., van Dishoeck E.F., 1994, *A&A* 283, 626
- Helmich F.P., van Dishoeck E.F., 1997, *A&AS* 124, 205
- Herbst E., 2000, In: Minh Y.C., van Dishoeck E.F. (eds.) *IAU Symposium 197, Astrochemistry: From Molecular Clouds to Planetary Systems*. ASP, p. 147
- Hogerheijde M.R., van der Tak F.F.S., 2000, *A&A* in press
- Hudson R.L., Moore M.H., 1999, *Icarus* 140, 451
- Johnston K.J., Gaume R., Stolovy S., et al., 1992, *ApJ* 385, 232
- Jones A.P., Tielens A.G.G.M., Hollenbach D.J., 1996, *ApJ* 469, 740
- Katz N., Furman I., Biham O., Pirronello V., Vidali G., 1999, *ApJ* 522, 305
- Keane J.V., Tielens A.G.G.M., Boogert A.C.A., Schutte W.A., Whittet D.C.B., 2000, *A&A* submitted
- Kerkhof O., Schutte W.A., Ehrenfreund P., 1999, *A&A* 346, 990
- Kurtz S., Cesaroni R., Churchwell E., Hofner P., Walmsley M., 2000, In: Mannings V.G., Boss A., Russell S.S. (eds.) *Protostars and Planets IV*, U. Arizona Press, p. 299
- Lahuis F., van Dishoeck E.F., 2000, *A&A* 355, 699
- Lee H.-H., Bettens R., Herbst E., 1996, *A&AS* 119, 111
- Lees R., Haque S., 1974, *Canadian J. Physics* 52, 2250
- MacDonald G.H., Thompson M.A., 2000, In: Minh Y.C., van Dishoeck E.F. (eds.) *IAU Symposium 197, Astrochemistry: From Molecular Clouds to Planetary Systems*. ASP, p. 113
- Mangum J.G., Wootten A., 1993, *ApJS* 89, 123
- Melnick G.J., 2000, In: Minh Y.C., van Dishoeck E.F. (eds.) *IAU Symposium 197, Astrochemistry: From Molecular Clouds to Planetary Systems*. ASP, p. 161
- Menten K.M., Walmsley C.M., Henkel C., Wilson T.L., 1986, *A&A* 157, 318
- Minier V., Booth R.S., Conway J.E., 1998, *A&A* 336, L5
- Ohishi M., 1997, In: van Dishoeck E.F. (ed.) *IAU Symposium 178, Molecules in Astrophysics - Probes and Processes*. Kluwer, Dordrecht, p. 61
- Padin S., Scott S.L., Woody D.P., Scoville N.Z., et al., 1991, *PASP* 103, 461
- Prasad S.S., Tarafdar S.P., 1983, *ApJ* 267, 603
- Rots A.H., Dickel H.R., Forster J.R., Goss W.M., 1981, *ApJ* 245, L15
- Sandford S.A., Allamandola L.J., 1993, *ApJ* 417, 815
- Schutte W.A., Boogert A.C.A., Tielens A.G.G.M., et al., 1999, *A&A* 343, 966
- Skinner C.J., Tielens A.G.G.M., Barlow M.J., Justtanont K., 1992, *ApJ* 399, L79
- Sobolev A.M., Cragg D.M., Godfrey P.D., 1997, *A&A* 324, 211
- Sutton E.C., Peng R., Danchi W.C., et al., 1995, *ApJS* 97, 455
- Takakuwa S., Mikami H., Saito M., 1998, *ApJ* 501, 723
- Thompson M.A., MacDonald G.H., 1999, *A&AS* 135, 531
- Tielens A.G.G.M., Allamandola L.J., 1987, In: Hollenbach D.J., Thronson H.A. Jr. (eds.) *Interstellar Processes*. *ASSL*, p. 397
- Tielens A.G.G.M., Hagen W., 1982, *A&A* 114, 245
- Tielens A.G.G.M., Tokunaga A.T., Geballe T.R., Baas F., 1991, *ApJ* 381, 181
- Turner B.E., 1990, *ApJ* 362, L29
- Turner B.E., 1998, *ApJ* 501, 731
- Vandenbussche B., Ehrenfreund P., Boogert A.C.A., et al., 1999, *A&A* 346, L57
- van der Tak F.F.S., van Dishoeck E.F., Evans N.J. II, Bakker E.J., Blake G.A., 1999, *ApJ* 522, 991
- van der Tak F.F.S., van Dishoeck E.F., Evans N.J. II, Blake G.A., 2000, *ApJ* 537, 283
- van Dishoeck E.F., Blake G.A., 1998, *ARA&A* 36, 317
- van Dishoeck E.F., Blake G.A., Jansen D. J., Groesbeck T.D., 1995, *ApJ* 447, 760
- van Dishoeck E.F., van der Tak F.F.S., 2000, In: Minh Y.C., van Dishoeck E.F. (eds.) *IAU Symposium 197, Astrochemistry: From Molecular Clouds to Planetary Systems*. ASP, p. 97
- Viti S., Williams D.A., 1999, *MNRAS* 305, 755
- Whittet D.C.B., Gerakines P.A., Tielens A.G.G.M., et al., 1998, *ApJ* 498, L159
- Wilson T.L., Walmsley C.M., Jewell P.R., Snyder L.E., 1984, *A&A* 134, L7
- Wright M.C.H., Plambeck R.L., Wilner D.J., 1996, *ApJ* 469, 216